Selective αv integrin depletion identifies a core, targetable molecular pathway that regulates fibrosis across solid organs

Neil C Henderson*, Thomas D Arnold, Yoshio Katamura, Marilyn M Giacomini, Juan D Rodriguez, Joseph H McCarty, Antonella Pellicoro, Elisabeth Raschperger, Christer Betsholtz, Peter G Ruminski, David W Griggs, Michael J Prinsen, Jacquelyn J Maher, John P Iredale, Adam Lacy-Hulbert, Ralf H Adams, Dean Sheppard*

*Address correspondence to: Neil Henderson (e-mail: Neil.Henderson@ed.ac.uk) or Dean Sheppard (e-mail: Dean.Sheppard@ucsf.edu).

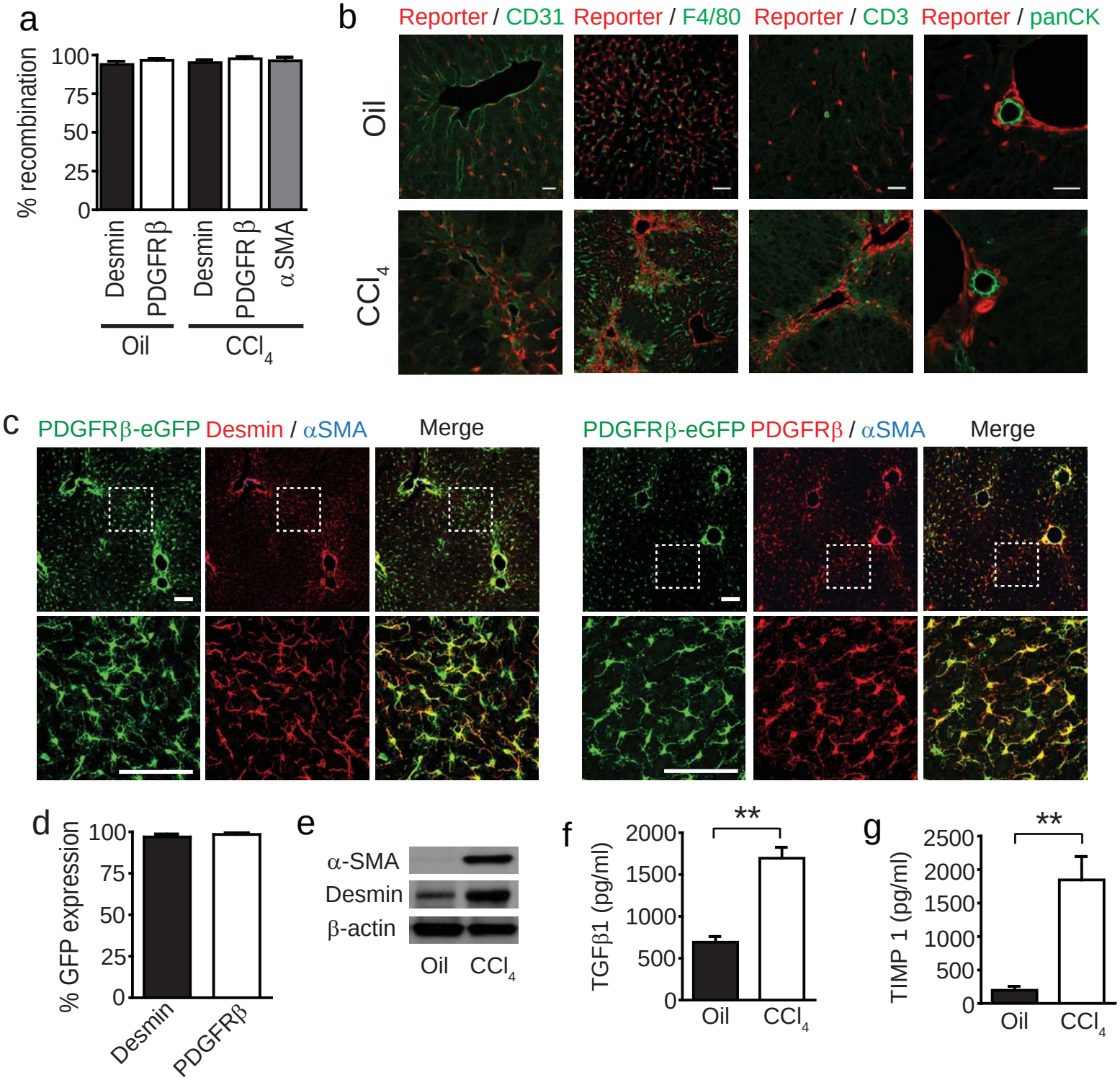

Supplementary Figure 1: *Pdgfrb*-Cre effectively targets recombination in HSC, quiescent mouse HSC express PDGFRβ, and analysis of protein expression in TdTomato positive cells sorted from Ai14;*Pdgfrb*-Cre reporter mice.

(**a**) Recombination efficiency in livers from control or chronic CCl_4 treated Ai14;*Pdgfrb*-Cre reporter mice ($n = 4$ male mice per group) stained for desmin, PDGFRβ or αSMA. (**b**) Immunofluoresence micrographs of liver sections from control (upper) or chronic CCl_4 treated (lower) Ai14;*Pdgfrb*-Cre reporter mice ($n = 4$ male mice per group) stained for endothelium (CD31, green), kupffer cells (F4/80, green), lymphocytes (CD3, green) and biliary epithelium (pan-cytokeratin, green) with endogenous Td tomato report in red. Scale bars, 25 µm (CD31, CD3 and pan-cytokeratin) and 50µm (F4/80). (**c**) Immunofluoresence micrographs of liver sections from uninjured *Pdgfrb*-BAC-eGFP reporter mice ($n = 4$ male mice) stained for desmin and PDGFRβ (red), αSMA (blue) and endogenous *Pdgfrb*-BAC-eGFP report in green. Lower panels are higher-magnification insets from boxed areas in upper panels. Scale bars, 100 µm. (**d**) Recombination efficiency in uninjured livers from *Pdgfrb*-BAC-eGFP mice. (**e**) Western blotting of αSMA and desmin expression in freshly sorted Td tomato positive cells from control or chronic CCl_4 treated Ai14;*Pdgfrb*-Cre mice. (**f,g**) Total TGF-β1 and TIMP1 concentrations in cell lysates from freshly sorted Td tomato positive cells from control or chronic CCl_4 treated Ai14;*Pdgfrb*-Cre mice. $n = 4$ male mice per group. Data are mean ± s.e.m. $^{**}P < 0.01$ (Student's *t* test).

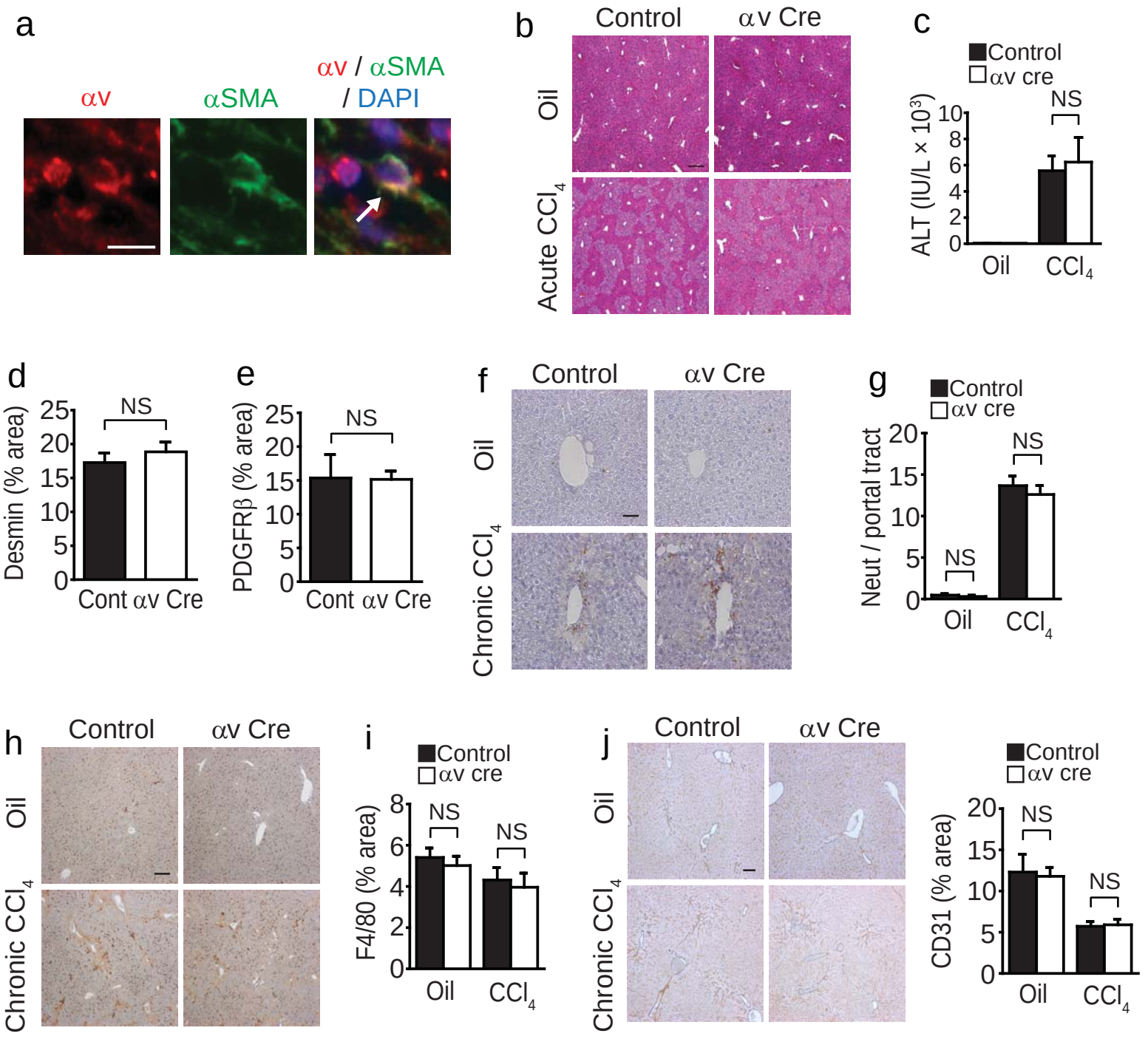

Supplementary Figure 2: Hepatic myofibroblasts express αv integrin in human fibrotic liver tissue, and αv integrin depletion on murine HSCs does not affect initial liver injury after CCl_4 treatment, baseline HSC number, inflammatory infiltrates or the vasculature of *itgav*$^{flox/flox}$;*Pdgfrb*-Cre livers.

(**a**) Representative immunofluorescence micrographs of human fibrotic liver tissue stained for αv integrin (red), αSMA (green) and DAPI (blue) (n = 5 cases). Arrow (right panel) indicates αv integrin and αSMA double-positive cell. Scale bar, 10 μm. (**b**) Micrographs of hematoxylin / eosin stained liver sections from control or *itgav*$^{flox/flox}$;*Pdgfrb*-Cre (αv Cre) mice 24 h after a single i.p. injection of olive oil or CCl_4 (n = 6 male mice per group). Scale bar, 200μm. (**c**) Serum alanine aminotransferase (ALT) levels. (**d,e**) Digital image analysis of desmin and PDGFRβ staining in uninjured control and *itgav*$^{flox/flox}$;*Pdgfrb*-Cre livers (n = 6 male mice per group). (**f**) Gr1 immunohistochemistry of liver tissue after control or chronic CCl_4 treatment of control and *itgav*$^{flox/flox}$;*Pdgfrb*-Cre mice. (n = 8 male mice per group). Scale bar, 50μm. (**g**) Neutrophil counting. (**h**) F4/80 immunohistochemistry of liver tissue after control or chronic CCl_4 treatment of control and *itgav*$^{flox/flox}$;*Pdgfrb*-Cre mice. Scale bar, 200μm. (**i**) Digital image analysis quantification of F4/80 staining. (**j**) CD31 immunohistochemistry of liver tissue (left) after control or chronic CCl_4 treatment of control and *itgav*$^{flox/flox}$;*Pdgfrb*-Cre mice. Scale bar, 100μm. Digital image analysis quantification of CD31 staining (right). Data are mean ± s.e.m. (Student's t test).

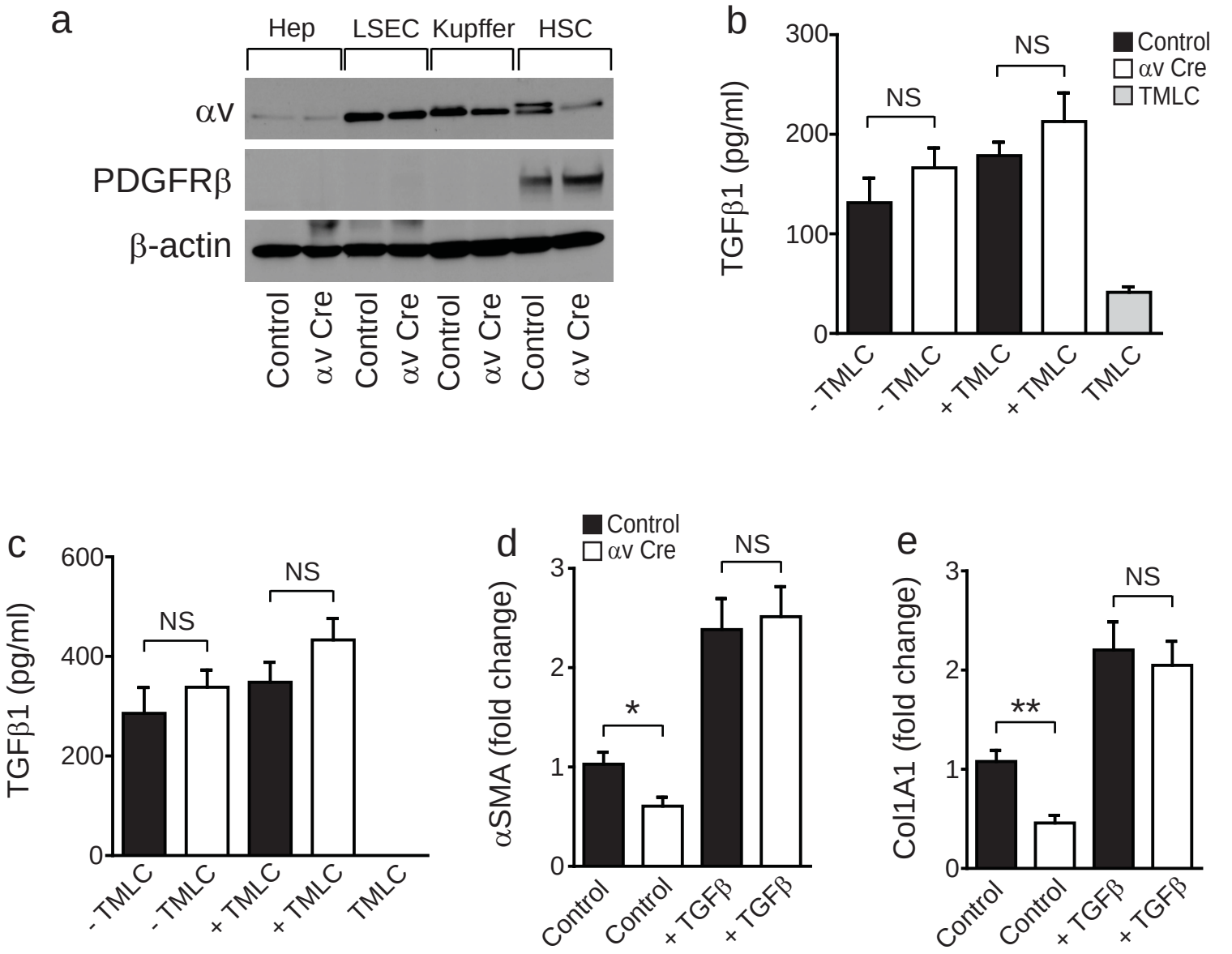

Supplementary Figure 3: αv integrin and PDGFRβ expression in purified hepatic cell populations from *itgav*$^{flox/flox}$;*Pdgfrb*-Cre mice, total TGF-β1 concentrations in control and *itgav*$^{flox/flox}$;*Pdgfrb*-Cre HSCs, and addition of TGF-β1 to *itgav*$^{flox/flox}$;*Pdgfrb*-Cre HSCs rescues pro-fibrotic gene expression.

(**a**) Western blotting of αv integrin and PDGFRβ expression in purified hepatocytes (Hep), liver sinusoidal endothelial cells (LSECs), kupffer cells and HSCs from control and *itgav*$^{flox/flox}$;*Pdgfrb*-Cre (αv Cre) male mice 5 days post isolation. (**b**) Total TGF-β1 concentrations measured by ELISA in cell lysates from control and *itgav*$^{flox/flox}$;*Pdgfrb*-Cre HSCs cultured with and without TMLCs (**c**) Total TGF-β1 concentrations measured by ELISA in supernatants from control and *itgav*$^{flox/flox}$;*Pdgfrb*-Cre HSCs cultured with and without TMLCs. (**d**) qPCR analysis of αSMA expression in control and *itgav*$^{flox/flox}$;*Pdgfrb*-Cre (αv Cre) HSCs treated with control or recombinant TGF-β1 (1ng ml^{-1}) for 24 h. (**e**) qPCR analysis of *Col1A1* expression in control and *itgav*$^{flox/flox}$;*Pdgfrb*-Cre (αv Cre) HSCs treated with control or recombinant TGF-β1 (1ng ml^{-1}) for 24 h. Data are mean ± s.e.m. *P < 0.05, **P < 0.01 (Student's *t* test).

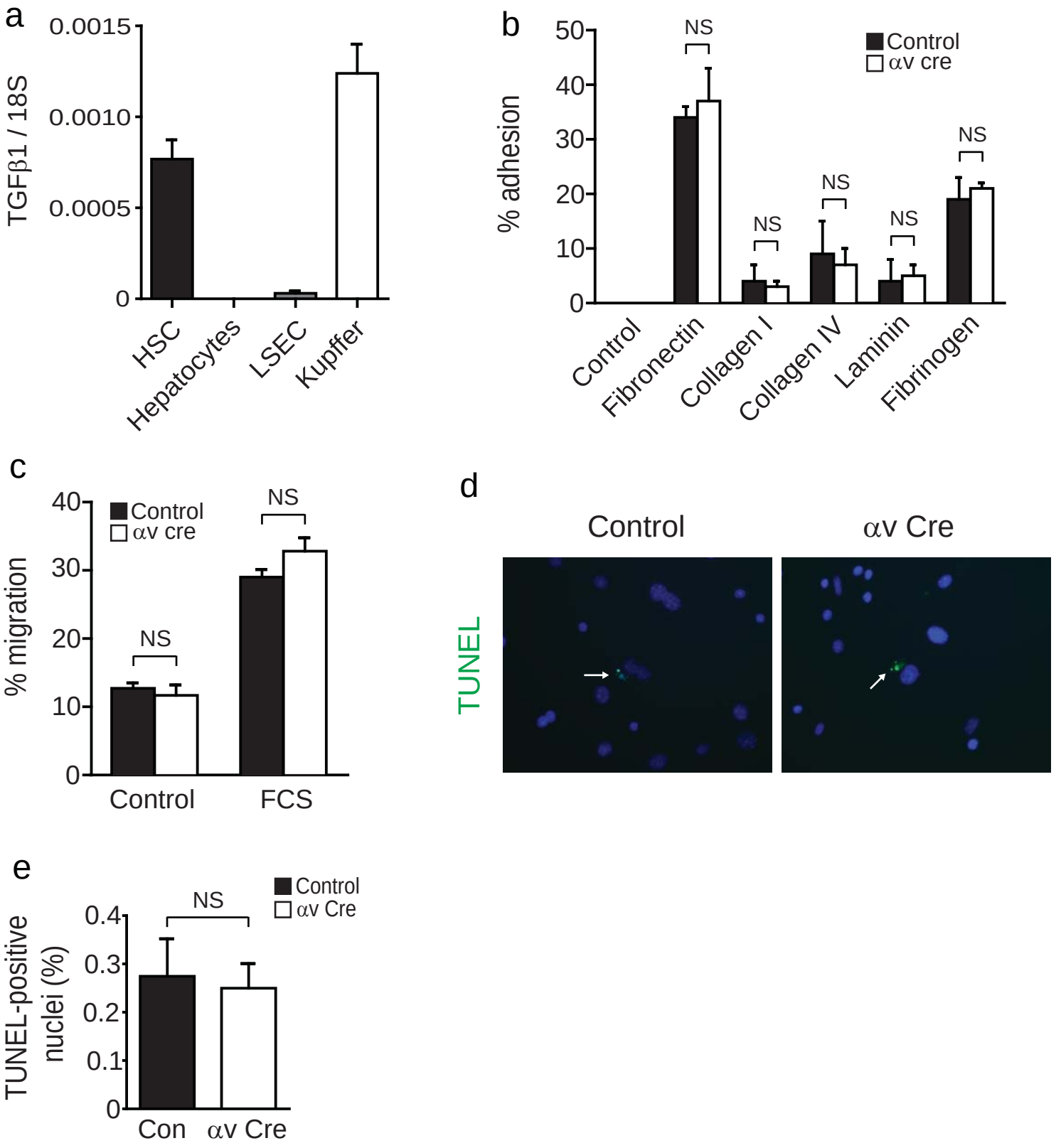

Supplementary Figure 4: TGF-β1 expression in hepatic cell populations isolated from CCl_4-induced fibrotic liver, and assessment of adhesion, migration and anoikis in control and *itgav*$^{flox/flox}$;*Pdgfrb*-Cre HSCs.
(**a**) qPCR analysis of *TGFb1* mRNA expression in purified HSCs, hepatocytes, liver sinusoidal endothelial cells (LSECs) and kupffer cells isolated from CCl_4-induced fibrotic livers (n = 4 male mice per group). (**b**) Adhesion assay of control and *itgav*$^{flox/flox}$;*Pdgfrb*-Cre HSCs plated on different matrices. (**c**) Migration assay of control and *itgav*$^{flox/flox}$;*Pdgfrb*-Cre HSCs (**d**) TUNEL immunofluorescence staining of control and *itgav*$^{flox/flox}$;*Pdgfrb*-Cre HSCs. Arrows indicate TUNEL positive nuclei (green), DAPI (blue). (**e**) Quantitation of TUNEL-positive nuclei. Data are mean ± s.e.m. (Student's *t* test).

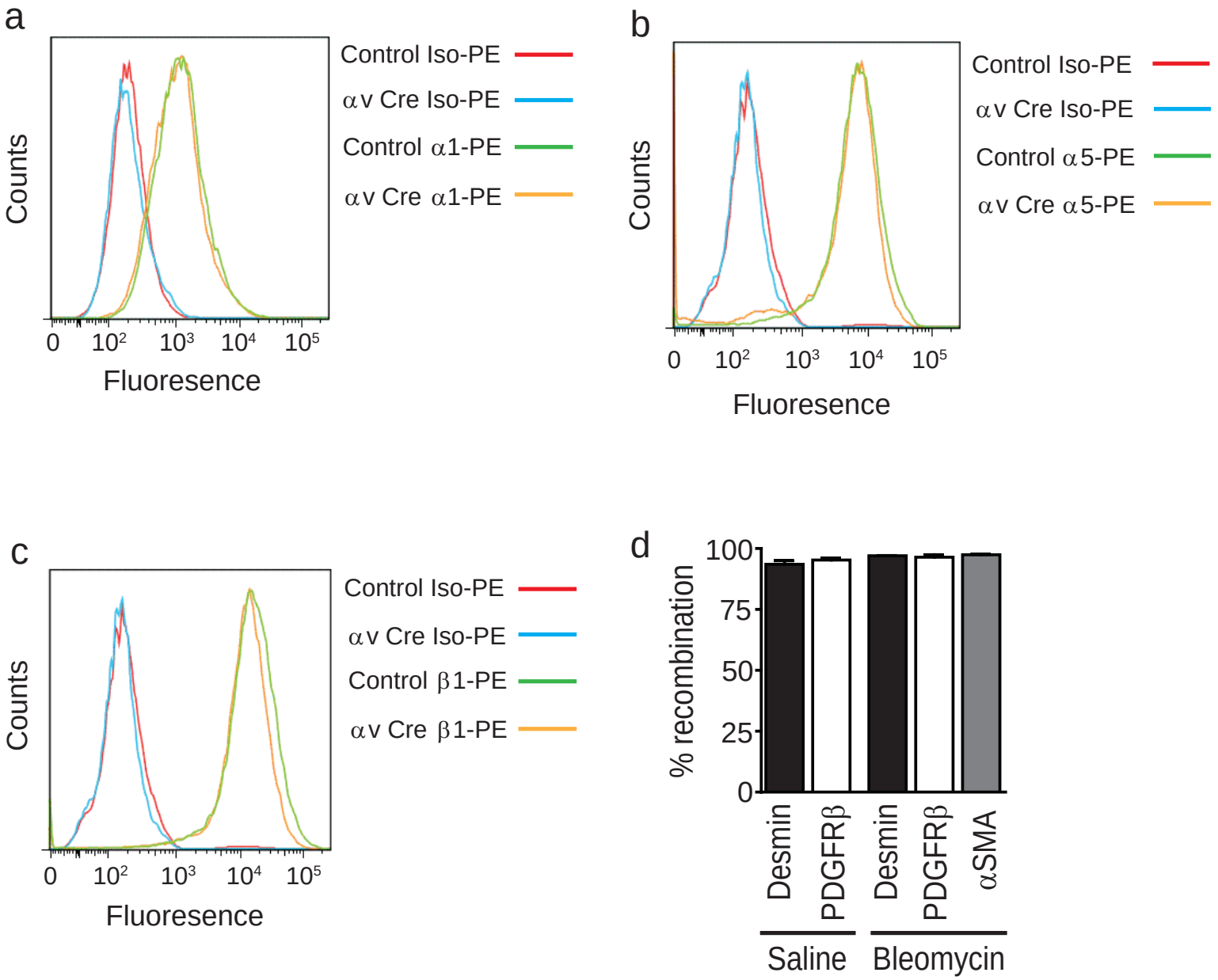

Supplementary Figure 5: FACS analysis of α1, α5 and β1 integrin expression levels in control and *itgav*$^{flox/flox}$;*Pdgfrb*-Cre HSCs, and recombination efficiency in lung pericytes and myofibroblasts in Ai14;*Pdgfrb*-Cre mice.

FACS analysis of (**a**) α1, (**b**) α5 and (**c**) β1 integrin expression levels in control and *itgav*$^{flox/flox}$;*Pdgfrb*-Cre HSCs cultured on tissue culture plastic for 5 days. (**d**) Analysis of recombination efficiency in lungs from saline treated (control) or bleomycin treated Ai14;*Pdgfrb*-Cre reporter mice ($n = 4$ male mice per group) stained for desmin, PDGFRβ or αSMA. Data are mean ± s.e.m.

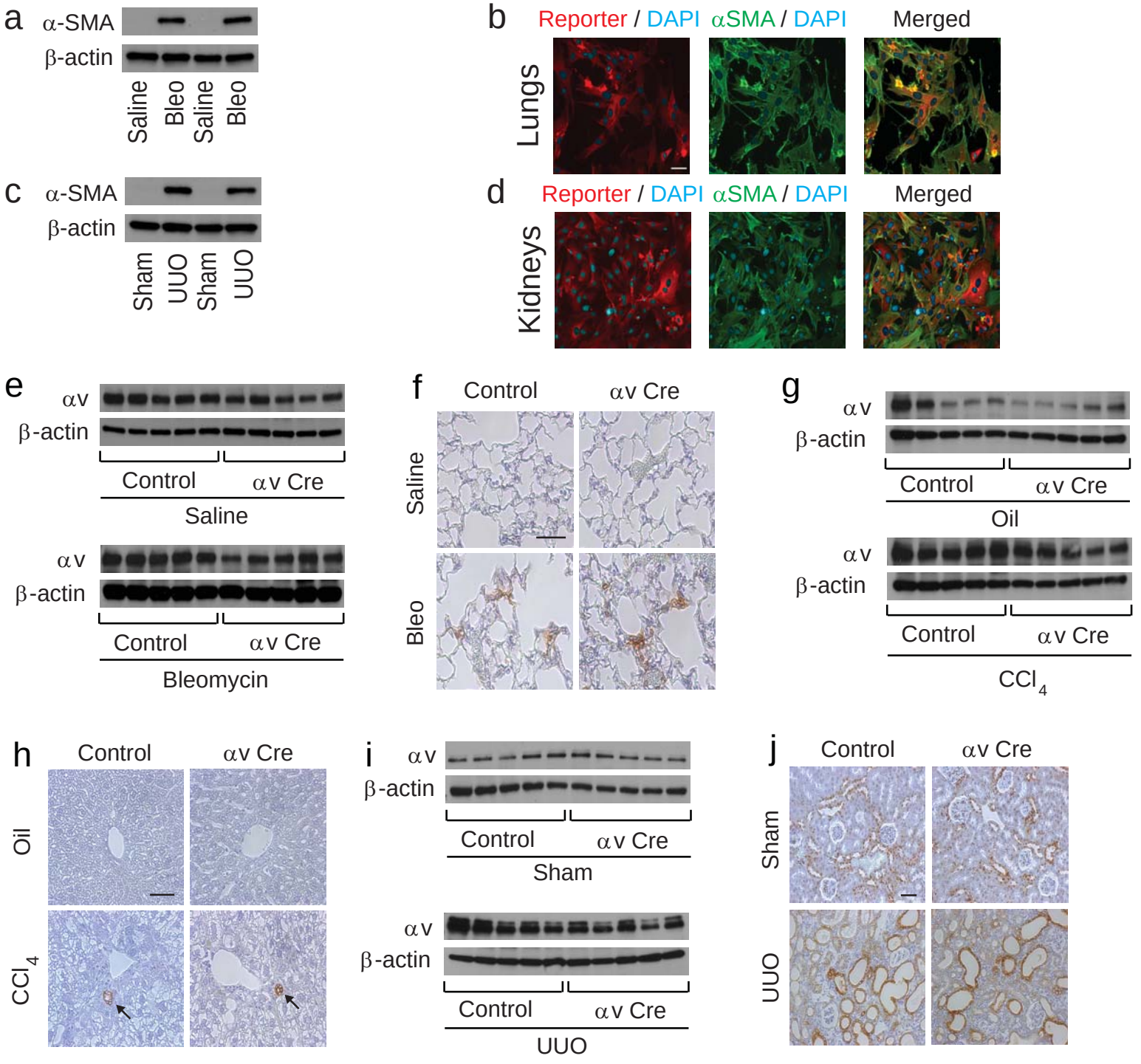

Supplementary Figure 6: Myofibroblast induction in Ai14-Td tomato positive cells sorted from lungs and kidneys of Ai14;*Pdgfrb*-Cre mice, and analysis of αv and β6 integrin expression in uninjured and fibrotic lung, liver and kidney in control and *itgav*$^{flox/flox}$;*Pdgfrb*-Cre mice. (**a**) Western blotting of αSMA in freshly sorted Td tomato positive cells from saline or bleomycin treated (28 days post instillation) Ai14;*Pdgfrb*-Cre mice ($n = 4$ male mice per group). (**b**) Immunofluoresence staining of Td tomato positive cells sorted from the uninjured lungs of Ai14;*Pdgfrb*-Cre mice and plated on tissue culture plastic for 7 days. Endogenous report (red), αSMA (green), DAPI (blue). Scale bar, 100μm. (**c**) Western blotting of αSMA in freshly sorted Td tomato positive cells from sham operated or UUO (day 7) Ai14;*Pdgfrb*-Cre mice ($n = 4$ male mice per group). (**d**) Immunofluoresence staining of Td tomato positive cells sorted from the uninjured kidneys of Ai14;*Pdgfrb*-Cre mice and plated on tissue culture plastic for 7 days. (**e**) Western blotting of αv expression in whole lung homogenates from saline or bleomycin treated control and *itgav*$^{flox/flox}$;*Pdgfrb*-Cre (αv Cre) mice. $n = 5$ male mice per group. (**f**) Representative sections of αvβ6 immunohistochemistry in lungs from saline or bleomycin treated control and *itgav*$^{flox/flox}$;*Pdgfrb*-Cre (αv Cre) mice. Scale bar, 50 μm. (**g**) Western blotting of αv expression in whole liver homogenates from olive oil or CCl_4 treated control and *itgav*$^{flox/flox}$;*Pdgfrb*-Cre (αv Cre) mice. $n = 5$ male mice per group. (**h**) Representative sections of αvβ6 immunohistochemistry in livers from olive oil or CCl_4 treated control and *itgav*$^{flox/flox}$;*Pdgfrb*-Cre (αv Cre) mice. Arrows indicate αvβ6 positive biliary epithelium. Scale bar, 50 μm. (**i**) Western blotting of αv expression in whole kidney homogenates from sham operated or UUO (day 14) control and *itgav*$^{flox/flox}$;*Pdgfrb*-Cre (αv Cre) mice. $n = 5$ male mice per group. (**j**) Representative sections of αvβ6 immunohistochemistry in kidneys from sham operated or UUO (day 14) control and *itgav*$^{flox/flox}$;*Pdgfrb*-Cre (αv Cre) mice. Scale bar, 50 μm.

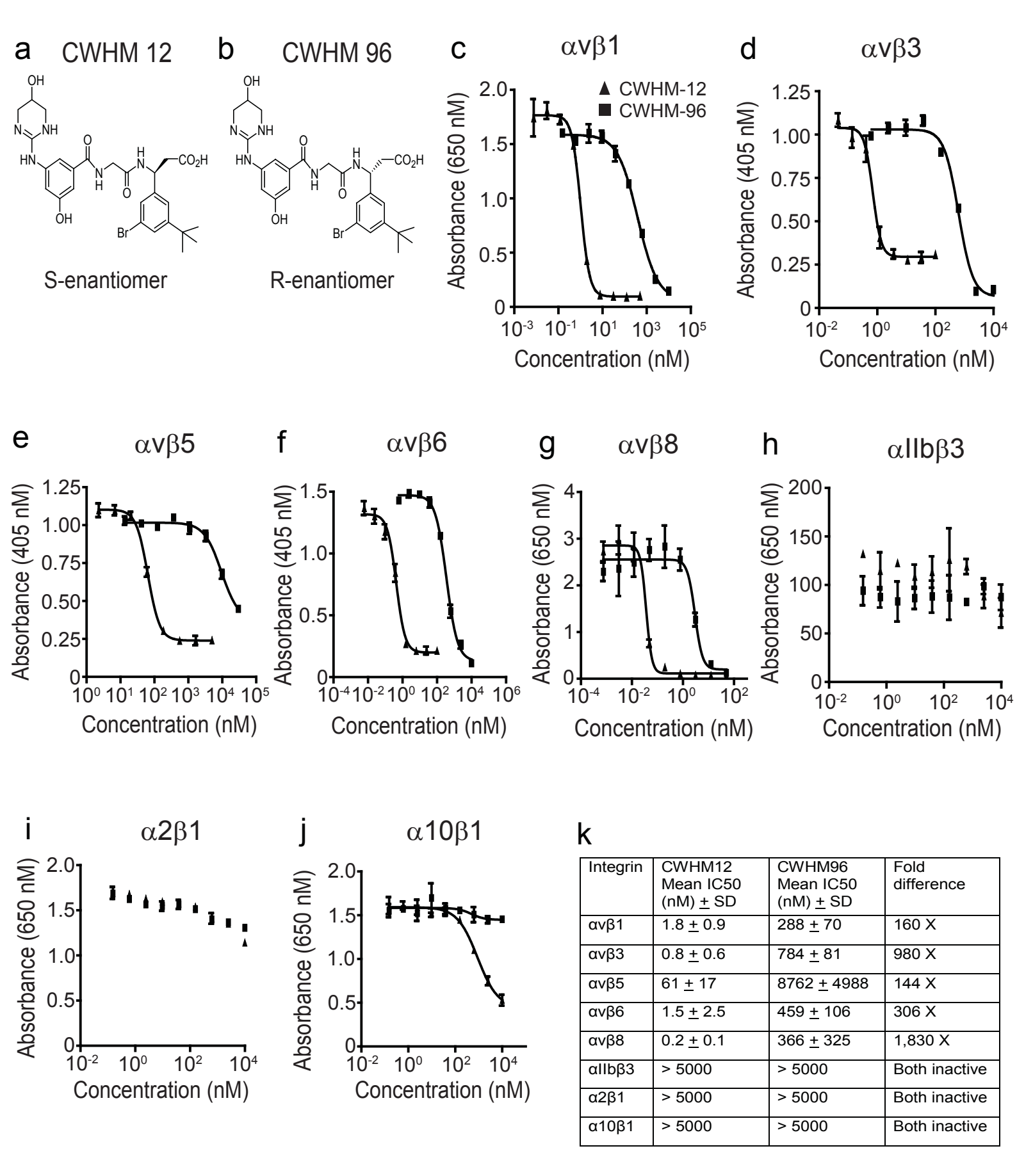

k

Integrin	CWHM12 Mean IC50 (nM) ± SD	CWHM96 Mean IC50 (nM) ± SD	Fold difference
αvβ1	1.8 ± 0.9	288 ± 70	160 X
αvβ3	0.8 ± 0.6	784 ± 81	980 X
αvβ5	61 ± 17	8762 ± 4988	144 X
αvβ6	1.5 ± 2.5	459 ± 106	306 X
αvβ8	0.2 ± 0.1	366 ± 325	1,830 X
αIIbβ3	> 5000	> 5000	Both inactive
α2β1	> 5000	> 5000	Both inactive
α10β1	> 5000	> 5000	Both inactive

Supplementary Figure 7: Inhibition of αv integrins by the novel small molecule CWHM 12.
(**a**) Chemical structure of CWHM 12. (**b**) Chemical structure of CWHM 96 (control R-enantiomer of CWHM 12). (**c–g**) Ligand-binding functions of αvβ1, αvβ3, αvβ5, αvβ6 and αvβ8 were measured as described in Materials and Methods. Representative CWHM 12 and CWHM 96 inhibition curves are shown for each assay. (**h–j**) Ligand-binding functions of αIIbβ3, α2β1 and α10β1 were measured as described in Materials and Methods. Representative CWHM 12 and CWHM 96 inhibition curves are shown for each assay. (**k**) Mean IC50 values and standard deviation from at least two identical experiments are summarized.

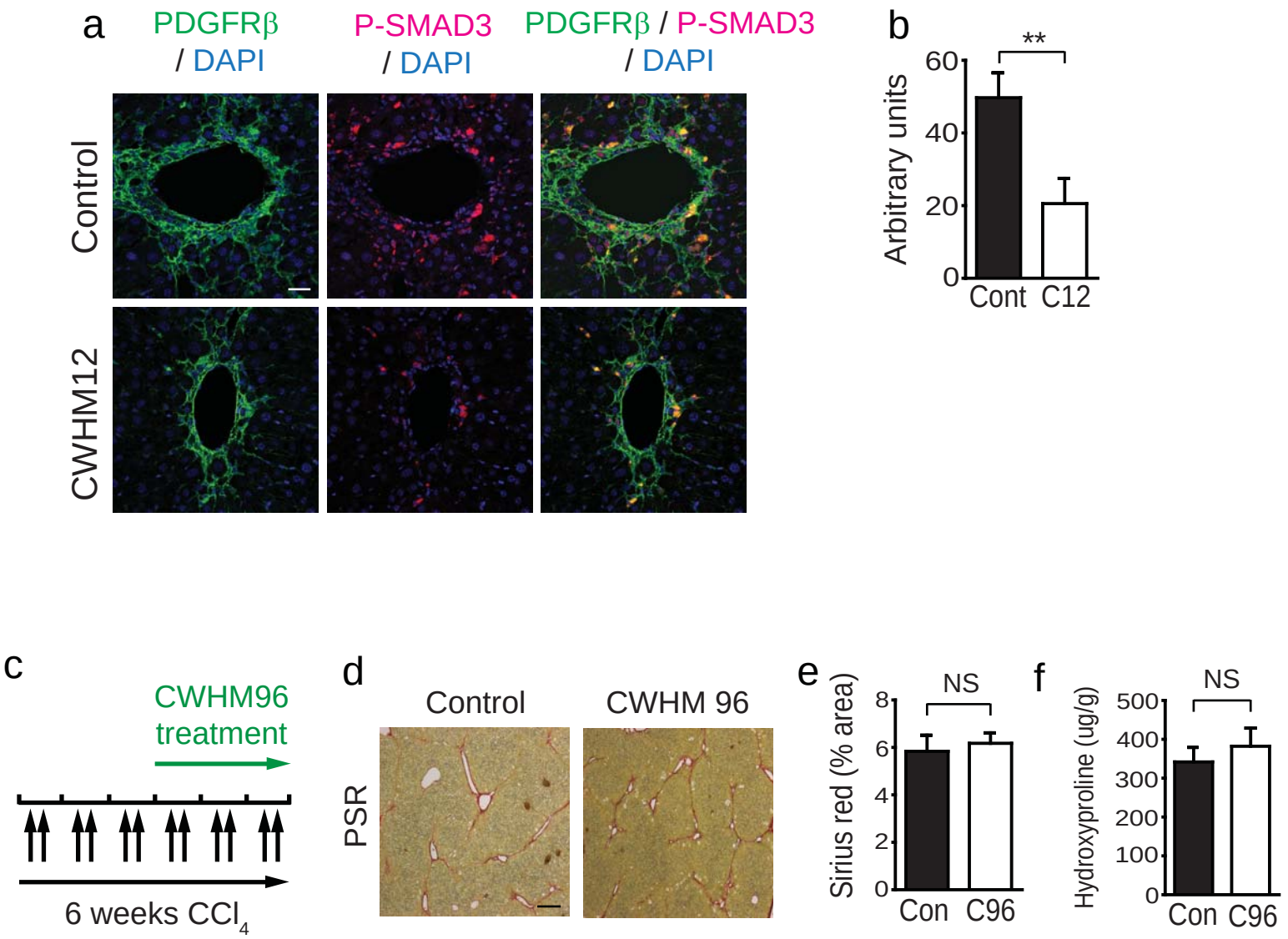

Supplementary Figure 8: Phospho-SMAD3 signaling is reduced in the livers of CWHM 12 treated mice following chronic CCl_4 administration, and treatment with CWHM 96 (control R-enantiomer of CWHM 12) does not inhibit liver fibrosis.

(**a**) Immunofluoresence micrographs of liver sections from control and CWHM 12 treated mice following chronic CCl_4 treatment (n =14 male mice per group). Scale bar, 25 μm. (**b**) Digital image analysis quantification of phospho-SMAD3 staining. (**c**) Dosing regime in the CWHM 96 (control R-enantiomer of CWHM 12) liver fibrosis model. Mice were given CCl_4 I.P. twice weekly for 3 weeks, then Alzet osmotic minipumps containing either CWHM 96 or vehicle (50% DMSO) were inserted, followed by a further 3 weeks of CCl_4 I.P. twice weekly. (**d**) Picrosirius red staining of liver tissue from vehicle control and CWHM 96 treated mice (n =10 male mice per group) after chronic CCl_4 treatment. Scale bar, 200μm. (**e**) Digital image analysis quantification of collagen (picrosirius red) staining. (**f**) Hydroxyproline analysis. Data are mean ± s.e.m. **P < 0.01 (Student's t test).